Controlled Lithium Dendrite Growth by a Synergistic Effect of Multilayered Graphene Coating and an Electrolyte Additive

ARTICLE *in* CHEMISTRY OF MATERIALS · APRIL 2015

Impact Factor: 8.35 · DOI: 10.1021/cm503447u

4 AUTHORS, INCLUDING:

Joo-Seong Kim
Korea Advanced Institute of Science and Tech…
19 PUBLICATIONS **288** CITATIONS
SEE PROFILE

Dae Woo Kim
Korea Advanced Institute of Science and Tech…
27 PUBLICATIONS **342** CITATIONS
SEE PROFILE

Jang Wook Choi
Korea Advanced Institute of Science and Tech…
115 PUBLICATIONS **6,405** CITATIONS
SEE PROFILE

CHEMISTRY OF MATERIALS

Article

pubs.acs.org/cm

Controlled Lithium Dendrite Growth by a Synergistic Effect of Multilayered Graphene Coating and an Electrolyte Additive

Joo-Seong Kim,[†,‡,∥] Dae Woo Kim,[§,∥] Hee Tae Jung,[*,§] and Jang Wook Choi[*,†,‡]

[†]Graduate School of Energy, Environment, Water, and Sustainability (EEWS) and [‡]Center for Nature-inspired Technology (CNiT), KAIST Institute NanoCentury, [§]Department of Chemical and Biomolecular Engineering, Korea Advanced Institute of Science and Technology (KAIST), 291 Daehakro, Yuseong-gu, Daejeon 305-701, Republic of Korea

Supporting Information

ABSTRACT: Lithium (Li) metal is the most ideal anode material in lithium ion batteries due to its large theoretical capacity (3860 mAh g^{-1}) and low redox potential (−3.04 V vs standard hydrogen potential, H_2/H^+). Nevertheless, surface dendrite formation during repeated charge−discharge cycles limits the cycle life and thus its practical use. The research efforts engaging polymer/ceramic coating or electrolyte additives have made noticeable progress, but further improvement is still desirable. Here, we report significantly improved performance by a synergistic effect of multilayered graphene (MLG) coating and Cs^+ additive in the electrolyte. MLG separates solid-electrolyte-interphase (SEI) formation from Li dendrites and thus stabilizes Coulombic efficiency in each cycle. Cs ions facilitate efficient interlayer diffusion of Li ions by enlarging the interlayer distance of MLG and also assists further for suppression of Li dendrite growth by electrostatic repulsion against Li ions. When paired with a stable sulfur−carbon composite electrode as a high capacity cathode, the Li−sulfur cell delivers an areal capacity of 4.0 mAh cm^{-2}, a value comparable to those of current commercial lithium ion batteries, with 81.0% capacity retention after 200 cycles.

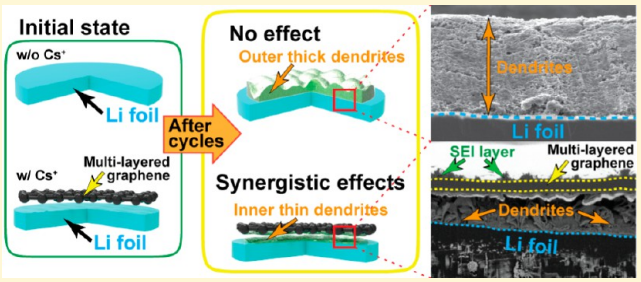

1. INTRODUCTION

Li metal has great advantages as an anode material in lithium ion batteries (LIBs). It has the unprecedentedly high theoretical capacity of 3860 mAh g^{-1} and a low redox potential (−3.04 V vs standard hydrogen potential, H_2/H^+).[1−7] Thus, Li metal could play a critical role in meeting the ever-growing demand on higher energy density in LIB operations, particularly targeting emerging applications represented by electrified vehicles and advanced portable electronic devices. Despite such attractive features associated with the capacity and the operating voltage, even decades of research has not yet fully addressed the longstanding drawback of the Li metal anode,[1,3,4,8] namely uncontrolled dendrite formation, leaving a substantial gap before its practical use. The lagging progress in resolving this chronic issue with the Li metal anode would also become a serious bottleneck in the timely advent of upcoming high energy density rechargeable batteries, such as Li−sulfur and Li−air cells.

Due to the high reactivity of Li metal with most electrolytes, the Li dendrite growth keeps on decomposing the electrolyte and forming solid-electrolyte-interphase (SEI) layers[9] on the Li surface over repeated cycles, leading to increased interfacial resistance and poor Coulombic efficiencies (CEs). After successive decomposition, the electrolyte could also be eventually exhausted. Furthermore, the Li dendrite growth could cause a severe fire hazard by generating internal short-circuits between both electrodes. The very challenge in handling the Li dendrite growth is that the Li dendrites could start even from microscopic roughness on the Li surface.[1−5,8,10] During electrochemical processes, electrons tend to be accumulated preferentially at the ridges of the microscopic roughness and thereafter promote more concentrated Li deposition at those spots from incoming Li ions. Hence, once the Li dendrite growth passes the very initial stage, the continuous growth is spontaneous and very difficult to stop. The limited success by using polymer electrolytes[11−15] can be explained in the same line that Li dendrites could grow through any microscopic open space between the polymer backbones as long as there exists the innate surface roughness on the starting Li metal. The use of ceramic solid electrolytes has turned out to be more effective in suppressing the Li dendrite growth,[16,17] but often gives rise to poor electrode−electrolyte contacts and consequently large interfacial resistances. The ceramic electrolytes also require additional steps accompanying more energy and cost.

Herein, we report a substantially improved cycling performance of Li metal anodes by a combined effect of multilayered graphene (MLG) coating (Figure 1a) and a large monovalent ion additive, namely the cesium ion (Cs^+). In this system, the main motivation of using MLG is to separate SEI layer

Received: September 18, 2014
Revised: March 20, 2015

DOI: 10.1021/cm503447u
Chem. Mater. XXXX, XXX, XXX−XXX

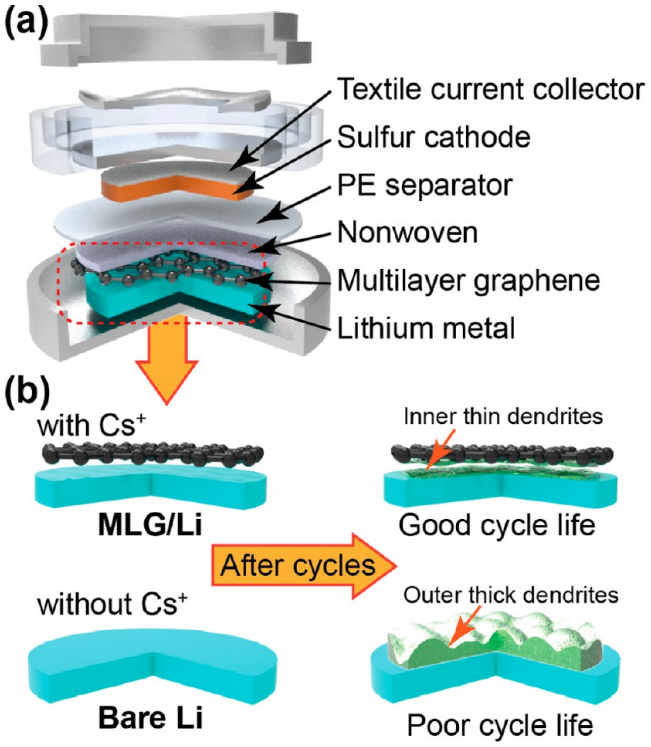

Figure 1. (a) A graphical illustration of cell configuration containing MLG and a nonwoven layer. (b) Different Li dendrite growth phenomena depending on the presence of Cs ions and MLG.

formation from Li dendrites by limiting SEI layers on the opposite side of MLG and thus to mitigate continuous decomposition of electrolyte on the Li dendrite surfaces. The MLG also keeps Li dendrites from growing beyond the MLG and therefore avoids internal short-circuits. MLG is a proper choice in fulfilling these functions because it can physically block micrometer dimension Li dendrites beyond its position while allowing for facile Li ion diffusion through its interlayered ionic channels. Furthermore, Cs ions were included in the electrolyte to enlarge the channel spacing in the MLG and thus to enhance Li ion diffusion. Due to the latter feature, Cs ions play a critical role in suppressing Li dendrite growth on the top surface of MLG, in addition to their known effect against Li dendrite growth by competitive electrostatic repulsion with Li ions.[3] These combined effects mitigate Li dendrite growth substantially and therefore make a sharp contrast against bare Li metal case (Figure 1b).

2. EXPERIMENTAL SECTION

Multilayered Graphene (MLG) Growth by Chemical Vapor Deposition (CVD) Process. Growth of MLG was conducted using conventional atmosphere pressure chemical vapor deposition. Ni foil (GoodFellow Co.) with a 25 μm thickness was inserted in a 4-in. thermal furnace and then annealed to 1000 °C under an Ar (500 sccm) and H_2 (50 sccm) environment. CH_4 gas (50 sccm) was injected while maintaining the flow of Ar and H_2 at 1000 °C for 1 h. As soon as the CH_4 injection was stopped, the thermal furnace was rapidly cooled down to room temperature, resulting in segregation of carbon atoms, and MLG was successfully prepared.

MLG Transfer Process. Because graphene can be grown on both sides of Ni foil, graphene on one side was etched using O_2 plasma (80 mW, 20 min). A poly methyl methacrylate (PMMA) supporing layer (10 wt % in chlorobenzene) was spin-coated at 3000 rpm on the MLG/Ni, and Ni foil was then etched using 1 M iron(III) chloride ($FeCl_3$) aqueous solution. After rinsing the MLG with DI water several times, MLG was transferred onto a nonwoven membrane and dried inside an oven at 60 °C. Next, the PMMA supporting layer was removed with acetone before a transfer of the MLG-nonwoven assembly to the Li foil (Honjo Chemical Co.).

Cell Preparation and Electrochemical Testing. Li−Li symmetrical cells were prepared by pairing bare Cu foil with Li metal in 2032 coin-type cells in an argon-filled glovebox. A polyethylene separator (SK innovation Co., Ltd.) was used as a separator. For convenience, MLG-on-Li electrode, MLG-on-Li electrode with cesium nitrate ($CsNO_3$) in the electrolyte, and MLG-free Li electrode with $CsNO_3$ in the electrolyte are denoted as MLG/Li, Cs-MLG/Li, and Cs-bare Li, respectively. In preparation of electrolytes, 1.05 M LiTFSI was used for bare Li and MLG/Li, and 1 M LiTFSI and 0.05 M $CsNO_3$ were used for Cs-MLG/Li and Cs-bare Li. All of the electrolytes were dissolved in cosolvents of DOL/DME (1:1 = v/v, PANAX ETEC, Korea). The sulfur electrode, carbonized polyacrylonitrile (PAN)-sulfur, namely *c*-PANS, used for Li−S cells was prepared following the reported procedure,[18,19] and its detailed preparation procedure is described in the Supporting Information. In the electrochemical measurements of the symmetric cells, the discharging process (Li deposition on Cu electrode) has a constraint capacity of 1 mAh cm^{-2}, and the end of the charge was set by a top cutoff voltage at 2 V vs Li/Li^+. Both processes were conducted using a battery cycler (MACCOR series 4000). The testing of the Li−S cells was carried out in the potential range of 1.0−3.0 V (vs Li/Li^+) at different current densities. In each cycle, discharge and charge were galvanostatically scanned under the constant current (CC) mode.

Characterizaiton of MLG before and after Ion Intercalation. Visualization of the domain structure of MLG was conducted by first coating the 4-cyano-4-pentylbipheny (5CB) liquid crystals with a thickness below 2 μm. Textures of the liquid crystals were then observed using a polarized optical microscope (POM; LV-100POL, Nikon) equipped with a hot stage (LT350, Linkam) and a charge-coupled device (CCD) camera. Raman spectra of MLG were attained using dispersive-Raman (ARAMIS, Horiba Jobin Yvon) with laser sources of excitation wavelength of 514 nm. The crystal structures of the pristine MLG and fully lithiated Cs-free MLG and Cs-containing MLG on Li foil were characterized by X-ray diffraction (XRD, Cu Kα, Rigaku). To obtain elemental depth profiles, the magnetic sector secondary ion mass spectrometry (M-SIMS, CAMECA IMS 7f, O_2^+, 10 kV, 100 nA) technique was used. The microscopic morphologies of MLG and Li metal before and after electrochmical processes were characterized by field emission scanning electorn microscopy (FE-SEM, Sirion). Elemental mapping was carried out by energy-dispersive X-ray spectroscopy (EDS) attached to the FE-SEM. To determine Li ion diffusivity and charge transfer resistance, electrochemical impedance spectroscopy (EIS, Bio-Logic) was conducted in the frequency range of 0.01 to 10^6 Hz with an amplitude of 14.2 mV. For cross-sectional visualization, a focused ion beam (FIB, Helios Nanolab 450 F1) with a Ga ion beam was used to dissect the samples.

3. RESULTS AND DISCUSSION

The MLG transfer onto the Li metal surface was accomplished via a conventional wet transfer method (Figure 2a). Briefly, MLG was synthesized by chemical vapor deposition (CVD) method using nickel (Ni) foil as a catalytic substrate.[20] The substrates and nonwoven membrane before and after MLG growth and transfer as well as after full lithiation are displayed in Figures 2b and S1. The quality of the grown MLG was investigated by attaining Raman spectra as shown in Figure 2c. A sharp G-band around 1600 cm^{-1} and shouldered 2D-band around 2700 cm^{-1} indicate that the grown MLG was composed of well-ordered sp^2 domains with high crystallinity, and each graphene layer was well stacked, respectively. From the low intensity of the D band around 1300 cm^{-1}, defect formation with sp^3 bonding seems negligible, but its weak intensity can be attributed to the existence of grain boundaries of graphene sheets.[21] Figure 2d shows the SEM image of MLG on Ni foil

DOI: 10.1021/cm503447u
Chem. Mater. XXXX, XXX, XXX−XXX

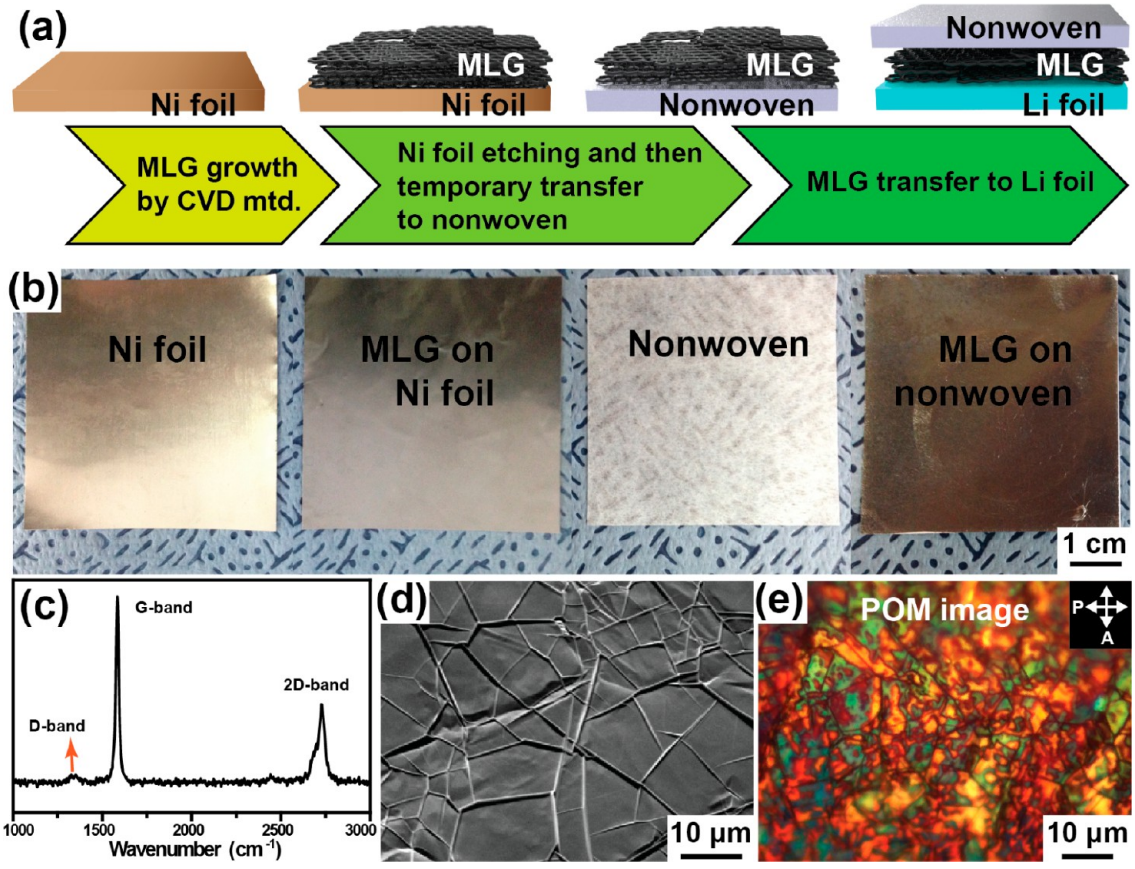

Figure 2. Growth, transfer, and characterization of MLG. (a) Schematic illustration showing MLG growth and its transfer to Li foil. (b) From left: bare Ni foil, MLG grown on Ni foil, bare nonwoven membrane, and MLG-transferred nonwoven membrane. (c) Raman spectrum of MLG. (d) SEM image of MLG on Ni foil showing graphene wrinkles. (e) Polarized optical microscope image of MLG on Ni foil. Each color piece indicates a single domain formed during the growth.

after the CVD growth. While wrinkled morphology caused by the different thermal expansion coefficients between Ni and graphene was observed, the full coverage of MLG on the surface of Ni foil was confirmed. Figure 2e displays the visualized domain structure of the prepared MLG by using polarized optical microscopy. In this analysis, each graphene domain was distinctively clarified by observing the liquid crystals aligned along the crystalline orientations of graphene domains.[22] Distinct birefringence colors, which are a result of the retardation of colors arising from interference between two components of polarized light split by the anisotropic liquid crystal molecules, indicate that MLG graphene was composed of a large number of sub-10-μm domains. Since graphene growth on Ni is mainly based on the segregation of dissolved carbon in Ni during the cooling process of CVD, it is expected that domains are mainly stacked or ascended over the next ones rather than merged into a single sheet.[23−26]

To elucidate the effect of the MLG coating in conjunction with electrolyte additive conditions on the electrochemical performance of the Li anode, symmetric cells in which Li metal and Cu foil are paired were tested. In this experiment, Li was deposited/dissolved onto/from the Cu foil in each cycle at a constant current of 1 mA cm^{-2}. The discharging process (Li deposition on Cu foil) was constrained by a constant lithiation capacity of 1 mAh cm^{-2}, whereas the end of the charging process was set by a top cutoff voltage at 2 V. The top-viewed morphology characterization (Figure 3) reflects the coating and additive effects, and the following points are noteworthy:

1. Bare Cu foil suffers from severe Li dendrite growth (Figure 3a). Li dendrites cover the entire area of Cu foil.

2. In the case of an MLG/Cu electrode without Cs^+ in the electrolyte, only a small amount of Li was found on the Cu surface (Figure 3b), which is attributed to poor Li diffusion through the interlayer spacing of the MLG. Instead, severe Li dendrite growth was observed on both sides of the MLG layer (Figure 3c).

3. By contrast, Cs-MLG/Cu showed far suppressed Li dendrite growth on the Cu surface (Figure 3d) and both sides of the MLG (Figure 3e). Dark spots (spot 1 of the SEM images in Figure 3d) were occasionally observed on the Cu surface and are ascribed to SEI formation according to EDS elemental analysis (Figure S2).[42] The bright spots (spot 2 of the SEM image in Figure 3d) were confirmed to be Cu from the EDS result (Figure S2). The significantly diminished dendrite growth on both sides of the MLG suggests the role of Cs ions that serve as pillars between the graphene layers of MLG and therefore facilitate Li ion interlayer diffusion. Due to the competitive situation between the top surface deposition and the interlayer diffusion, the improved interlayer diffusion reduces the Li dendrite growth on the top MLG surface substantially.

4. Cs-bare Cu foil also showed a certain level of Li dendrite growth (Figure 3f), reconfirming the synergistic effect of the MLG coating and the Cs additive in the case of Cs-MLG/Cu electrode.

DOI: 10.1021/cm503447u
Chem. Mater. XXXX, XXX, XXX−XXX

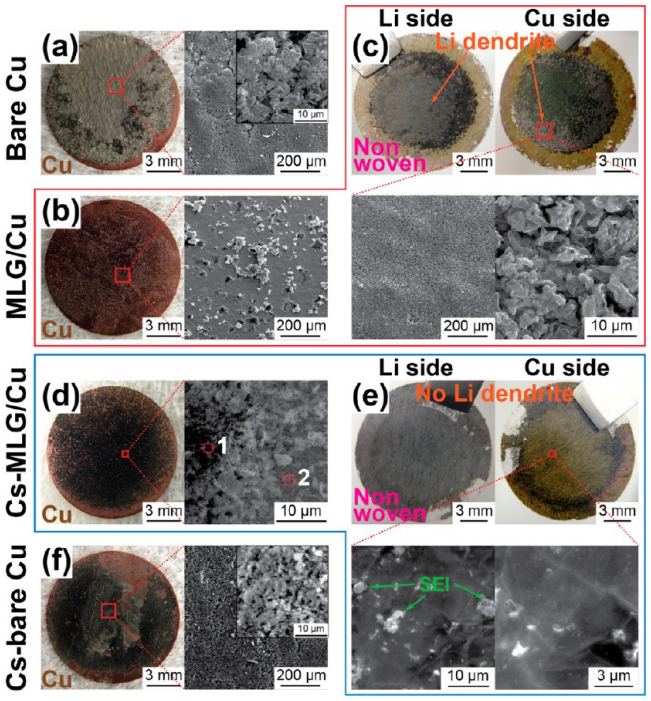

Figure 3. Surface characterization of symmetric cells after cycling. Digital camera and SEM images of top-viewed Cu electrode and MLG surfaces of the symmetric cells after 20 cycles. (a) Bare Cu foil after 20 cycles at charged state. (b) Cu surface of the MLG/Cu electrode after 20 cycles at charged state. (c) Both sides of the MLG of the same electrode after 20 cycles at charged state. (d) Cu surface of the Cs-MLG/Cu electrode after 20 cycles at charged state. (e) Both sides of the MLG of the same electrode. The bright spots indicative of SEI layers were occasionally observed on the top surface of the MLG coating layer. (f) Cs-bare Cu foil after 20 cycles at a charged state. All experiments were performed at 1 mA cm^{-2}.

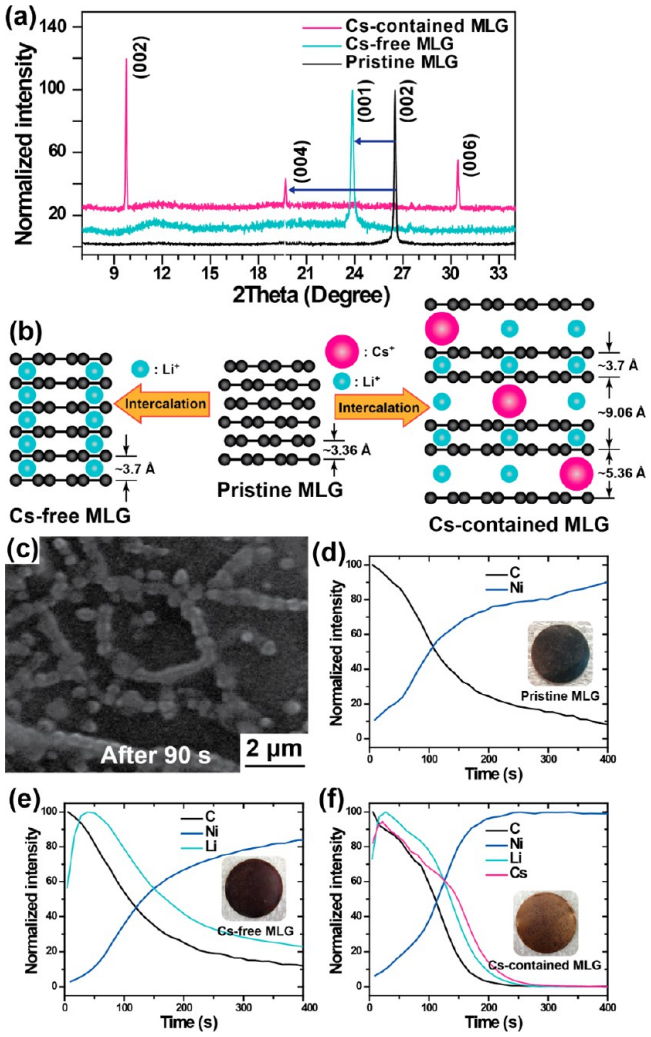

Figure 4. Cointercalation of Li and Cs ions into MLG. (a) XRD spectra of pristine MLG on Li foil, Cs-free MLG on Li foil after full discharge, and Cs-containing MLG on Li foil after full discharge. (b) Layered MLG structures after (left) Li intercalation and (right) Li/Cs cointercalation alongside the corresponding interlayer distances. (c) Surface SEM image of the Cs-containing MLG on Li foil after full discharge. The image was taken after ~90 s of air exposure. M-SIMS spectra of (d) pristine MLG, (e) Cs-free MLG after full discharge, and (f) Cs-containing MLG after full discharge.

The effect of Cs additive on the MLG structure was elucidated by characterizing MLG before and after ionic intercalation using X-ray diffraction (XRD) and magnetic sector secondary ion mass spectrometry (M-SIMS) analyses (Figure 4). For this, Li ions were galvanostatically intercalated into the MLG that was loaded on a nickel foil under a half-cell configuration in the presence and absence of Cs ions. The XRD peaks in the 2θ range of 7−34° (Figure 4a) provided the information on the interlayer distance of MLG after the ionic intercalation. The pristine MLG on Li foil exhibited a peak at 26.5° corresponding to the intrinsic (002) planes with an interlayer distance of 3.36 Å. After full lithiation (discharged at 5 mV vs Li/Li^+), Cs-free MLG showed a (001) peak shift to 23.9°, reflecting the increase in the interlayer distance to 3.7 Å after Li intercalation (left of Figure 4b). By contrast, after the same full lithiation, Cs-containing MLG showed three distinct peaks at 9.75°, 19.9°, and 30.2° assigned to the (002), (004), and (006) planes with corresponding interlayer distances of 9.06, 4.53, and 3.02 Å, respectively. The (002) plane with an interlayer distance of 9.06 Å originates from two adjacent Li and Li/Cs layers (right of Figure 4b). Interestingly, similar to the reported different stages of lithiated graphite[27,28] (Figure S3), i.e., LiC_6 (JCPDS 34-1320), LiC_{12} (JCPDS 35-1046), and LiC_{24} (JCPDS 35-1047), only the (002), (004), and (006) plane regularities were detected in the Cs-MLG/Li XRD spectrum, rather than those from the Li intercalated (3.7 Å) and the Li/Cs cointercalated (5.36 Å) layers. Also, the XRD spectrum of the fully lithiated Cs-containing MLG is very similar to that of stage II of only Li- or Cs-intercalated graphite (Figures S3−S5). However, its gold color after the cointercalation is reflective of stage I. This stage discrepancy can be resolved in a way that, as illustrated in Figures 4b and S5, Cs ions occupy every other layer, giving the XRD signature corresponding to stage II, but the Li layers in between the Li/Cs layers result in ionic intercalation into all the successive layers and thus the stage I color. Stage I of other similar intercalated compounds, such as LiC_6,[27−29] KC_8 (Figure S6),[29−31] and CsC_8,[29,32] also show a similar gold color. For reference, the structural configuration, interlayer distance, and chemical formulas of fully lithiated Cs-MLG/Li at different Cs amounts are suggested in Figure S5.

The Cs-containing MLG electrode was characterized after different times of air exposure using SEM after lithiation (Figures 4c and S7). The Cs-containing MLG showed CsO_x signals along lined particle patterns on the surface (see EDS

DOI: 10.1021/cm503447u
Chem. Mater. XXXX, XXX, XXX−XXX

results in Figure S8), whereas the Cs-free MLG did not show any such patterns at all. The discrete CsO_x signal seemingly indicates the entering points of Li and Cs intercalation. It has been known[33,34] that Cs intercalation into graphite is energetically more favorable than Li and Na intercalation because of more significant metal-to-carbon charge transfer that enhances the structural stability of the Cs-intercalated phases or equivalently lower ionization energy of Cs (3.89 eV vs 5.39 eV of Li or 5.14 eV of Na; Figure S9). In the same context, the preferred Cs intercalation can be interpreted in a way that the intercalated phases have higher stability and thus require less energy penalty in overcoming van der Waals interaction between graphene layers.[35] The entering points of Cs intercalation could be defective areas along the wrinkles (Figure 2d) as experimentally evidenced in the previous study.[36] However, as described above, in the current MLG, each domain edge is likely to expand and ascend over the adjacent domains.[23−25] Thus, Li intercalation in Cs-MLG/Li might be more predominant through the interlayer entrances at the crossings of adjacent domains, rather than the defective areas at the domain boundaries in the same graphene planes. Overall, Cs ions facilitate Li ion diffusion both between and across graphene layers and contribute to the diminished Li dendrite growth on the MLG top surface.

In addition, Li ion diffusion at the interface on the Cs-containing MLG electrode was superior, as semicircles indicative of charge transfer resistance (R_{ct}) became smaller in electrochemical impedance spectroscopy (EIS; Figure S10). In the EIS measurements, the Li ion diffusivity was obtained by using the equation in Figure S10c. For this, the Warburg slopes were attained from the EIS curves in the low frequency regime. The Li ion diffusivities (D_{Li}^{+}) of Cs-MLG/Li turned out to be 1−5 times higher than those of MLG/Li depending on the degree of lithiation, supporting enhanced Li interlayer diffusion via Cs additive. D_{Li}^{+} of MLG/Li was also consistent with the reported value of lithiated graphite.[37,38] On the other hand, the intercalation of Li ions or Li/Cs ions was further verified by M-SIMS analyses. While the as-produced MLG showed carbon and Ni depth profiles according to the presence of Cs^{+} (Figure 4f), it followed similar depth profiles to the carbon profiles, reconfirming the intercalation of these ions into MLG. The color changes from black to brownish (Figure 4e inset and S1) and gold (Figure 4f inset and S1) reflects the increased interlayer distances but to the different values depending on the intercalated ions. The thickness of MLG in the current investigation was determined for convenient handling of MLG during its transfer to Li metal. Even thinner MLG is expected to perform the same functions, as the main role of MLG is to offer bridging ionic channels to carrier ions before their reaching to the Li metal while isolating SEI layers from Li metal anode. The present MLG (∼100 nm) must be thin enough to be saturated with the carrier ions.

The distinct trend between the samples was also consistent with the Li dendrite growth observed over the cross-sections (Figure 5). Bare Cu (Figure 5a) and Cs-free MLG/Cu (Figure 5b) grew thick Li dendrite layers (115 and 88 μm, respectively) after 20 cycles in a charged state. In contrast, Cs-containing MLG/Cu showed dramatically decreased Li dendrite growth: almost negligible growth in the charged state after 20 cycles (Figure 5c) and only 6-μm-thick even in the discharged state after 40 cycles (Figure 5d). In the absence of MLG, Cs-bare Cu exhibited a thicker Li dendrite layer (51-μm-thick; Figure 5e),

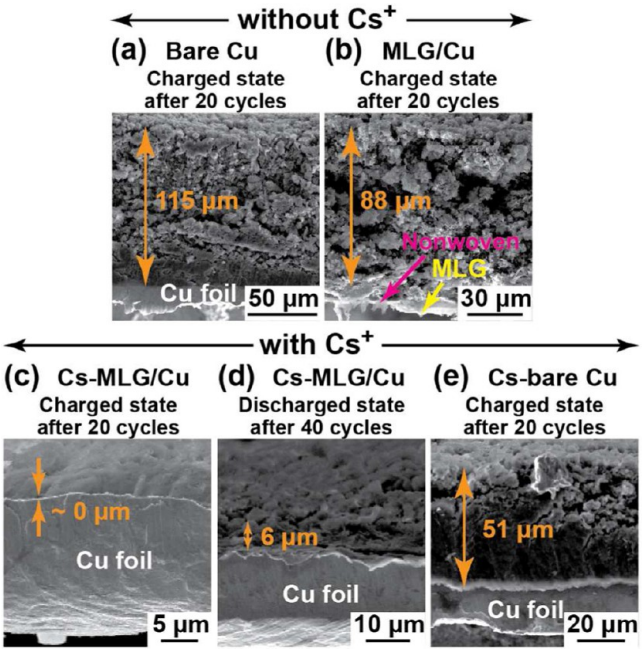

Figure 5. Cross-sectional SEM images of symmetric cells during cycling. (a) Bare Cu and (b) MLG/Cu without Cs^{+} after 20 cycles in the charged state. (c) Cs-MLG/Cu in the charged state after 20 cycles. (d) Cs-MLG/Cu in the discharged state after 40 cycles. (e) Cs-bare Cu in the charged state after 20 cycles.

reconfirming the importance of the synergistic effect between the MLG and the Cs additive.

The CEs during cycling reflect the critical MLG and additive effect among the given samples when tested under the symmetric configuration (Figure 6a). The CE was defined as charging capacity over discharging capacity (fixed to 1 mAh). While the CE of Cs-MLG/Cu was 90.6% after 50 cycles, the CEs of Cs-bare Cu, MLG/Cu, and bare Cu were lower at 71.8%, 47.5%, and 38.4% after the same number of cycles. The lower CEs can be understood in a way that, although a constant capacity of 1 mA cm^{-2} was applied to Li deposition, a certain portion of the capacity was consumed for side reactions on grown Li dendrites, and a smaller amount of Li is dissolved in the delithiation process in the same cycle, resulting in a smaller delithiation (charging) capacity. The potential profiles showing the distinct CEs are also presented in Figures 6b−e at different cycle numbers. At the first cycle, Cs-MLG/Cu exhibited larger overpotentials than those of the other samples (Figure 6b inset) due to the interlayer diffusion through the MLG. However, the trend becomes the opposite at the 44th cycle (Figure 6e inset), as interfacial resistance becomes larger for the other samples due to continuous SEI formation on the grown Li dendrites.

The synergistic effect between the MLG and the electrolyte additive was applied to a practical Li−S cell, as Li−S cells are required to resolve the Li dendrite problem for their stable operations. To this end, we chose *c*-PANS as a cathode material because *c*-PANS has proven[18,39,40] to deliver robust cycling in Li−sulfur batteries due to well-defined carbon−sulfur chemical bonds that alleviate fatal lithium polysulfides dissolution.

The cycling performance was examined for the Li−S cells with the different MLG coating and Cs additive conditions when cycled at 1.0 mA cm^{-2} (Figure 7a). The bare Li and MLG/Li cells exhibited sharp capacity fading even in the very beginning of the cycles, whereas the Cs-MLG/Li cell showed

DOI: 10.1021/cm503447u
Chem. Mater. XXXX, XXX, XXX−XXX

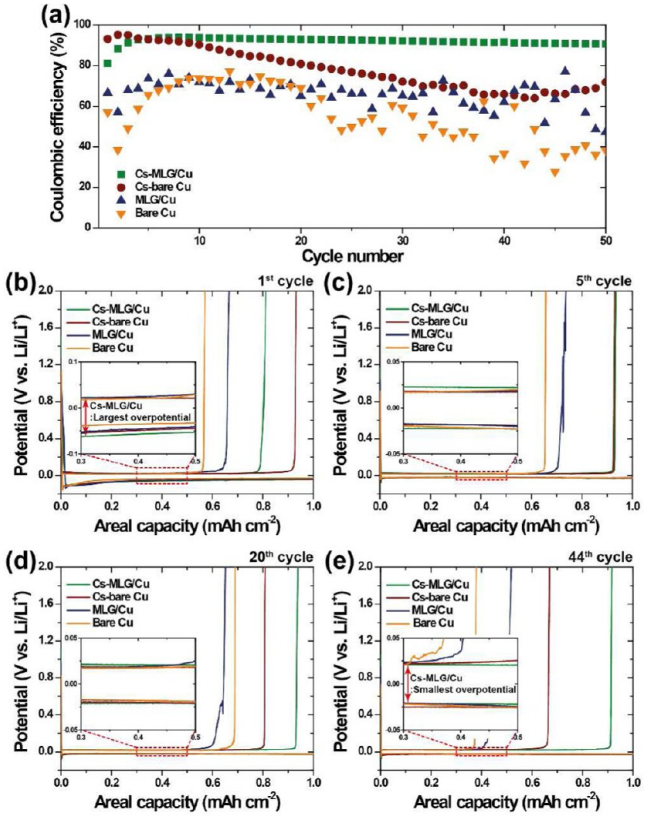

Figure 6. (a) Cycling performance of symmetric cells containing Cs-MLG/Cu, Cs-bare Cu, MLG/Cu, and bare Cu at 1.0 mA cm^{-2} and (b–e) their corresponding voltage profiles at different cycle numbers.

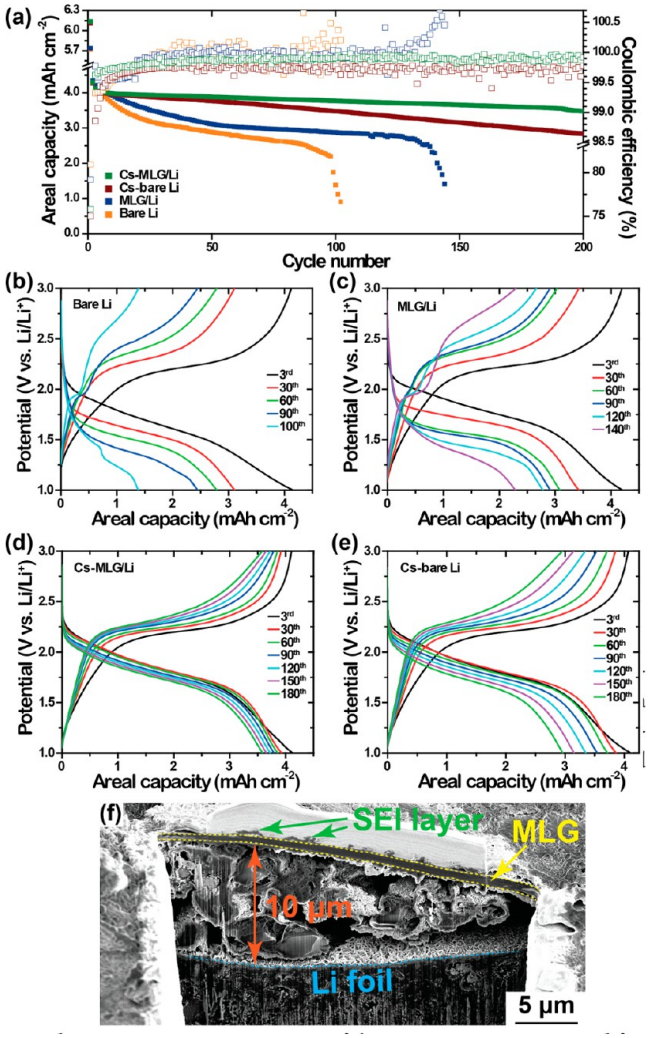

Figure 7. (a) Cycling performance of bare Li, MLG/Li, Cs-MLG/Li, and Cs-bare Li at 1.0 mA cm^{-2} and (b–e) their corresponding voltage profiles at different cycle numbers. (f) Cross-sectional SEM image of Cs-MLG/Li after 80 cycles at 1.0 mA cm^{-2}.

much more stable capacity retention. The Cs-bare Li cell showed better performance than the first two cells but worse performance than the Cs-MLG/Li cell. The MLG/Li cell showed a very similar capacity fading behavior to that of the bare Li cell, which is again attributed to the Li dendrite growth on the top MLG surface. In comparison, the Cs-MLG/Li cell showed superior capacity retentions of 90.4%, 87.7%, and 85.1% at the cycle numbers of 50, 100, and 150, respectively, with respect to the capacity in the secondary cycle. At the same cycling stages, the capacity retentions of the Cs-bare Li cell were 88.1%, 81.3%, and 73.7%, respectively. Notably, the capacity retentions of the Cs-MLG/Li cell were achieved at high areal capacity near 4.0 mAh cm^{-2}, the value comparable to those of commercial LIB cells, which suggests that the current approach can address the issue of Li dendrite growth at commercially viable areal capacities. Indeed, destabilized interfaces on Li dendrite surfaces were reflected in increased overpotentials in the discharge–charge profiles of the bare Li and MLG/Li cells with repeated cycles (Figures 7b and c), which are in contrast with far more persistent overpotentials of the Cs-MLG/Li cell (Figure 7d). As in the cycling performance, the Cs-bare Li cell showed intermediate performance (Figure 7e), as it showed smaller overpotentials than those of the bare Li and MLG/Li cells but larger overpotentials than those of the Cs-MLG/Li cell. In addition, it was observed that the electrolyte in most of the dead cells was dried out, suggesting that unstable interface associated with uncontrolled Li dendrite growth accelerates electrolyte consumption. In our experiment, for fair comparison, the same amount of 0.4 mL of the electrolyte was injected to each coin cell.

Also, the CE (=charge capacity/discharge capacity) is consistent with those of the symmetric cells in Figure 6a and provides useful information in understanding the electrochemical operations of each cell. The CEs of the bare Li and MLG/Li cells showed severe fluctuations and even values surpassing 100% intermittently during cycling. Similar to the Li–Li symmetric cells, the CEs over 100% are ascribed[19] to electrolyte decomposition on Li dendrite surfaces. In Li–S cells, the lithium polysulfide reaction with Li metal during charge could additionally increase the CE, as it could increase charge capacity. In the overall efficiency consideration, the lithiation/delithiation efficiency of the sulfur electrode could also affect the overall efficiency (as in normal half-cell tests). However, the lithiation/delithiation efficiency on the Li metal side must be farther away from 100% and thus more deterministic on the overall efficiency, as the Li dendrite growth at the given current densities is very serious. In contrast with the bare Li and MLG/Li cells, the Cs-MLG/Li cell exhibited stable CEs over repeated cycles. The average CEs in the cycle period of 1–200, 2–200, and 5–200 were 99.7%, 99.8%, and 99.9%, respectively.

DOI: 10.1021/cm503447u
Chem. Mater. XXXX, XXX, XXX–XXX

As displayed in Figure 7f, the Cs-MLG/Li cell after 80 cycles exhibited similar Li dendrite morphology to that after one cycle (Figures S11 and S12). Although the thickness of Li dendrites increased to 8−12 μm, it is remarkable that a majority of the SEI layers still remained isolated on the other side of MLG and Li dendrites show their own morphologies without significant coverage of SEI layers. The top-viewed and cross-sectional images after one cycle for the same Li−S cells are presented in Figures S11 and S12 and indicate that the cells without the synergistic effect suffered from severe Li dendrite growth even during the first cycle.

The effect of the MLG coating and the $CsNO_3$ additive can be summarized as follows and is also presented in a diagram in Figure 8:

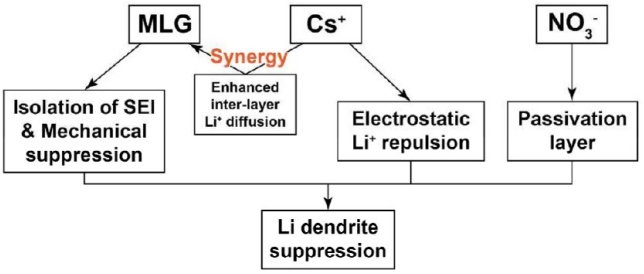

Figure 8. A diagram summarizing the effects of MLG coating and ions in the electrolyte.

1. The main role of the MLG coating is to isolate SEI layers from the Li metal surface, preventing successive side reactions on Li dendrites.

2. The MLG coating itself contributes further against the Li dendrite growth by applying the pressure onto the Li metal surface. For reference, single-layer graphene has been known[41] to have a very high Young's modulus reaching 1 TPa, and MLG has also been known[42] to have a higher values (0.5 TPa) than that (3.4−4.9 GPa[43,44]) of Li metal.

3. Cs^+ cointercalates with Li ions into the MLG and assists facile interdiffusion of Li ions.

4. Cs^+ suppresses Li dendrite growth at sharp tips of the Li surface via its electrostatic repulsion against incoming Li ions.

5. NO_3^- leads to formation of passivation layers that prohibit further unwanted reactions with electrolyte and polysulfides.[6,19,45]

4. CONCLUSION

In conclusion, by engaging a synergistic effect of MLG coating and Cs ion additive, we have demonstrated controlled surface dendrite growth of a Li metal anode during repeated cycles and have thus improved its cycling performance significantly. The key strategy of such treatment is to isolate the SEI formation from Li dendrites while Li diffusion to and from the Li surface is facilitated. The current approach enables achievement of robust cycling even at commercial-level areal capacities when paired with a high capacity sulfur electrode and could thus play a critical role in making lithium metal-based future rechargeable batteries, such as Li−S and Li−air cells, more competitive in practical cell settings.

■ ASSOCIATED CONTENT

Supporting Information

Digital photographs of the materials, XRD patterns of graphite at different lithiation states, illustration of inserted alkali metal into graphite, structure models and chemical formulas of cointercalated graphite, illustrations of color change in case of potassium, SEM image of cointercalated MLG, EDS characterization of cointercalated MLG, ionization potentials of the materials, and Li ion diffusivity calculation by EIS technique. Additional SEM images of sulfur electrodes. This material is available free of charge via the Internet at http://pubs.acs.org.

■ AUTHOR INFORMATION

Corresponding Authors

*E-mail: heetae@kaist.ac.kr.
*E-mail: jangwookchoi@kaist.ac.kr.

Author Contributions

‖The manuscript was written through contributions of all authors. All authors have given approval to the final version of the manuscript. These authors contributed equally.

Notes

The authors declare no competing financial interest.

■ ACKNOWLEDGMENTS

H.T.J. acknowledges the financial support by National Research Foundation of Korea (NRF-2015R1A2A1A05001844). J.W.C. acknowledges the financial support by the National Research Foundation of Korea (NRF) Grant funded by the Korea government (MEST; NRF-2010-C1AAA001-0029031, NRF-2012-R1A2A1A01011970, and NRF-2014R1A4A1003712).

■ REFERENCES

(1) Xu, W.; Wang, J.; Ding, F.; Chen, X.; Nasybulin, E.; Zhang, Y.; Zhang, J.-G. *Energy Environ. Sci.* **2014**, *7* (2), 513.
(2) Park, M. S.; Ma, S. B.; Lee, D. J.; Im, D.; Doo, S.-G.; Yamamoto, O. *Sci. Rep.* **2014**, *4*, 3815.
(3) Ding, F.; Xu, W.; Graff, G. L.; Zhang, J.; Sushko, M. L.; Chen, X.; Shao, Y.; Engelhard, M. H.; Nie, Z.; Xiao, J.; Liu, X.; Sushko, P. V.; Liu, J.; Zhang, J.-G. *J. Am. Chem. Soc.* **2013**, *135* (11), 4450.
(4) Ding, F.; Xu, W.; Chen, X.; Zhang, J.; Shao, Y.; Engelhard, M. H.; Zhang, Y.; Blake, T. A.; Graff, G. L.; Liu, X.; Zhang, J.-G. *J. Phys. Chem. C* **2014**, *118* (8), 4043.
(5) Nishida, T.; Nishikawa, K.; Rosso, M.; Fukunaka, Y. *Electrochim. Acta* **2013**, *100* (0), 333.
(6) Zheng, G.; Lee, S. W.; Liang, Z.; Lee, H.-W.; Yan, K.; Yao, H.; Wang, H.; Li, W.; Chu, S.; Cui, Y. *Nat. Nanotechnol.* **2014**, *9* (8), 618.
(7) Lu, Y.; Tu, Z.; Archer, L. A. *Nat. Mater.* **2014**, *13* (10), 961.
(8) Ryou, M.-H.; Lee, D. J.; Lee, J.-N.; Lee, Y. M.; Park, J.-K.; Choi, J. W. *Adv. Energy Mater.* **2012**, *2* (6), 645.
(9) Lv, D.; Shao, Y.; Lozano, T.; Bennett, W. D.; Graff, G. L.; Polzin, B.; Zhang, J.; Engelhard, M. H.; Saenz, N. T.; Henderson, W. A.; Bhattacharya, P.; Liu, J.; Xiao, J. *Adv. Energy Mater.* **2014**, 1400993.
(10) Aurbach, D.; Zinigrad, E.; Cohen, Y.; Teller, H. *Solid State Ionics* **2002**, *148* (3−4), 405.
(11) Croce, F.; Appetecchi, G. B.; Persi, L.; Scrosati, B. *Nature* **1998**, *394* (6692), 456.
(12) Bouchet, R.; Maria, S.; Meziane, R.; Aboulaich, A.; Lienafa, L.; Bonnet, J.-P.; Phan, T. N. T.; Bertin, D.; Gigmes, D.; Devaux, D.; Denoyel, R.; Armand, M. *Nat. Mater.* **2013**, *12* (5), 452.
(13) Tarascon, J. M.; Armand, M. *Nature* **2001**, *414* (6861), 359.
(14) Lee, S. H.; Harding, J. R.; Liu, D. S.; D'Arcy, J. M.; Shao-Horn, Y.; Hammond, P. T. *Chem. Mater.* **2014**, *26* (8), 2579.
(15) Khurana, R.; Schaefer, J. L.; Archer, L. A.; Coates, G. W. *J. Am. Chem. Soc.* **2014**, *136* (20), 7395.

DOI: 10.1021/cm503447u
Chem. Mater. XXXX, XXX, XXX−XXX

(16) Kim, S.-H.; Choi, K.-H.; Cho, S.-J.; Kil, E.-H.; Lee, S.-Y. *J. Mater. Chem. A* **2013**, *1* (16), 4949.
(17) Lee, Y.-S.; Lee, J. H.; Choi, J.-A.; Yoon, W. Y.; Kim, D.-W. *Adv. Funct. Mater.* **2013**, *23* (8), 1019.
(18) Hwang, T. H.; Jung, D. S.; Kim, J.-S.; Kim, B. G.; Choi, J. W. *Nano Lett.* **2013**, *13* (9), 4532.
(19) Kim, J.-S.; Hwang, T. H.; Kim, B. G.; Min, J.; Choi, J. W. *Adv. Funct. Mater.* **2014**, *6*, 5359.
(20) Kim, K. S.; Zhao, Y.; Jang, H.; Lee, S. Y.; Kim, J. M.; Kim, K. S.; Ahn, J.-H.; Kim, P.; Choi, J.-Y.; Hong, B. H. *Nature* **2009**, *457* (7230), 706.
(21) Ferrari, A. C.; Meyer, J. C.; Scardaci, V.; Casiraghi, C.; Lazzeri, M.; Mauri, F.; Piscanec, S.; Jiang, D.; Novoselov, K. S.; Roth, S.; Geim, A. K. *Phys. Rev. Lett.* **2006**, *97* (18), 187401.
(22) Kim, D. W.; Kim, Y. H.; Jeong, H. S.; Jung, H.-T. *Nat. Nanotechnol.* **2012**, *7* (1), 29.
(23) Li, X.; Cai, W.; Colombo, L.; Ruoff, R. S. *Nano Lett.* **2009**, *9* (12), 4268.
(24) Reina, A.; Jia, X.; Ho, J.; Nezich, D.; Son, H.; Bulovic, V.; Dresselhaus, M. S.; Kong, J. *Nano Lett.* **2008**, *9* (1), 30.
(25) Kim, S. J.; Kim, D. W.; Jung, H.-T. *RSC Adv.* **2013**, *3* (45), 22909.
(26) Yu, Q.; Lian, J.; Siriponglert, S.; Li, H.; Chen, Y. P.; Pei, S.-S. *Appl. Phys. Lett.* 2008, *93*, 11.
(27) Ohzuku, T.; Iwakoshi, Y.; Sawai, K. *J. Electrochem. Soc.* **1993**, *140* (9), 2490.
(28) Sacci, R. L.; Adamczyk, L. A.; Veith, G. M.; Dudney, N. J. *J. Electrochem. Soc.* **2014**, *161* (4), A614.
(29) Dresselhaus, M. S.; Dresselhaus, G. *Adv. Phys.* **2002**, *51* (1), 1.
(30) Wang, Y.; Puech, P.; Gerber, I.; Pénicaud, A. *J. Raman Spectrosc.* **2014**, *45* (3), 219.
(31) Lovell, A. *Tuneable graphite intercalates for hydrogen storage*. Ph. D. thesis, University Colleage London, 2007.
(32) Rey, N.; Toulemonde, P.; Machon, D.; Duclaux, L.; Le Floch, S.; Pischedda, V.; Itié, J. P.; Flank, A. M.; Lagarde, P.; Crichton, W. A.; Mezouar, M.; Strässle, T.; Sheptyakov, D.; Montagnac, G.; San-Miguel, A. *Phys. Rev. B* **2008**, *77* (12), 125433.
(33) Kawaguchi, M.; Kurasaki, A. *Chem. Commun.* **2012**, *48* (55), 6897.
(34) LeeEduardo, J. H.; Balasubramanian, K.; Weitz, R. T.; Burghard, M.; Kern, K. *Nat. Nanotechnol.* **2008**, *3* (8), 486.
(35) Wang, Z.; Selbach, S. M.; Grande, T. *RSC Adv.* **2014**, *4* (8), 4069.
(36) Petrović, M.; Šrut Rakić, I.; Runte, S.; Busse, C.; Sadowski, J. T.; Lazić, P.; Pletikosić, I.; Pan, Z. H.; Milun, M.; Pervan, P.; Atodiresei, N.; Brako, R.; Šokčević, D.; Valla, T.; Michely, T.; Kralj, M. *Nat. Commun.* **2013**, *4*, 2772.
(37) Takami, N.; Satoh, A.; Hara, M.; Ohsaki, T. *J. Electrochem. Soc.* **1995**, *142* (2), 371.
(38) Persson, K.; Sethuraman, V. A.; Hardwick, L. J.; Hinuma, Y.; Meng, Y. S.; van der Ven, A.; Srinivasan, V.; Kostecki, R.; Ceder, G. *J. Phys. Chem. Lett.* **2010**, *1* (8), 1176.
(39) Wang, J.; Yang, J.; Xie, J.; Xu, N. *Adv. Mater.* **2002**, *14* (13−14), 963.
(40) Yin, L.; Wang, J.; Lin, F.; Yang, J.; Nuli, Y. *Energy Environ. Sci.* **2012**, *5* (5), 6966.
(41) Lee, C.; Wei, X.; Kysar, J. W.; Hone, J. *Science* **2008**, *321*, 5887.
(42) Frank, I. W.; Tanenbaum, D. M.; van der Zande, A. M.; McEuen, P. L. *J. Vac. Sci. Technol. B* **2007**, *25*, 6.
(43) Monroe, C.; Newman, J. *J. Electrochem. Soc.* **2005**, *152*, 2.
(44) Yan, K.; Lee, H.-W.; Gao, T.; Zheng, G.; Yao, H.; Wang, H.; Lu, Z.; Zhou, Y.; Liang, Z.; Liu, Z.; Chu, S.; Cui, Y. *Nano Lett.* **2014**, *14*, 10.
(45) Zheng, G.; Yang, Y.; Cha, J. J.; Hong, S. S.; Cui, Y. *Nano Lett.* **2011**, *11* (10), 4462.

DOI: 10.1021/cm503447u
Chem. Mater. XXXX, XXX, XXX−XXX